An approximate technique for analyzing the plasma of thermionic converters operating in the ignited mode*

Manuel Ratafia* and James C. Keck

Department of Mechanical Engineering, Massachusetts Institute of Technology, Cambridge, Massachusetts 02139
(Received 21 March 1974)

An approximate analytic technique for solving the transport equations of thermionic energy converters is developed. Using an assumed parametric form for the ionization rate, the problem is reduced, essentially, to one of the solution of three simultaneous transcendental equations. A numerical iterative procedure for the solution of these equations is derived and implemented in a computer code and some illustrative solutions are obtained. A simple criterion for whether the converter is operating under equilibrium or nonequilibrium conditions and other simple relations describing the character of the solutions are derived. For nonequilibrium conditions, the assumed form for the ionization rate is found to agree well with the actual form, and the solutions obtained are in good agreement with previous results. The empirically observed minimum in the arc drop at the optimum value of the pressure-spacing product is predicted. The present theory is the only one known to the authors which shows this result. The solutions may be systematically improved by numerical integration and iteration and the range of applicability of the solutions can be extended to local thermodynamic equilibrium conditions by assuming a more general form for the electron production and to a greater variation in parameters by incorporating a recently derived improved set of boundary conditions into the analysis.

I. INTRODUCTION

Various forms of essentially the same transport equations and various associated boundary conditions describing the plasma of thermionic converters operating in the ignited mode have been derived in the past. A typical form for the transport equations is that of Wilkins and Gyftopoulos[1] and boundary conditions similar to those used in the present study are employed by McCandless *et al.*[2] To solve these equations it is necessary to integrate the relation for the net ionization rate distribution across the converter.

Previous analytical attempts at integrating the transport equations employ approximations which limit their applicability to values of the product of the pressure and interelectrode spacing which are much greater than those of interest for power-producing converters. The numerical "shooting" methods, typified by the work of McCandless *et al.*[2] and of Wilkins and McCandless,[3] on the other hand, are subject to numerical instabilities which make them exceedingly expensive and difficult to implement; in addition they provide relatively little physical insight into the phenomena involved.

In this study, by assuming a parametric form for the ionization rate distribution across the converter and adjusting the parameters so as to fit the assumed form to the actual one, the transport equations are integrated analytically and thereby reduced to a set of three simultaneous transcendental equations. These equations are solved numerically by means of an iterative method in a computer program.

Comparison of the assumed and calculated forms of the ionization rate distribution show the form assumed here to be successful for small values of the pressure-spacing product which corresponds to nonequilibrium conditions. These are the conditions of interest for practical converters. Solutions applicable to research converters, which have larger pressure-spacing products, can be obtained, using our method, by means of a more general assumed form for the ionization rate. Such a form can be obtained by a superposition of two forms of the type assumed here.

The formulation of the problem in terms of a set of equations to be solved is presented in Sec. II. In Sec. III the transport equations are integrated, and in Sec. IV the numerical methods of solution of the integrated equations are described. In Sec. V some solutions are presented and discussed and conclusions are drawn.

II. MATHEMATICAL FORMULATION

A. Physical model

As is indicated in Fig. 1(a), the interelectrode space of the converter is considered in terms of three regions consisting of a plasma region bounded by two sheaths of

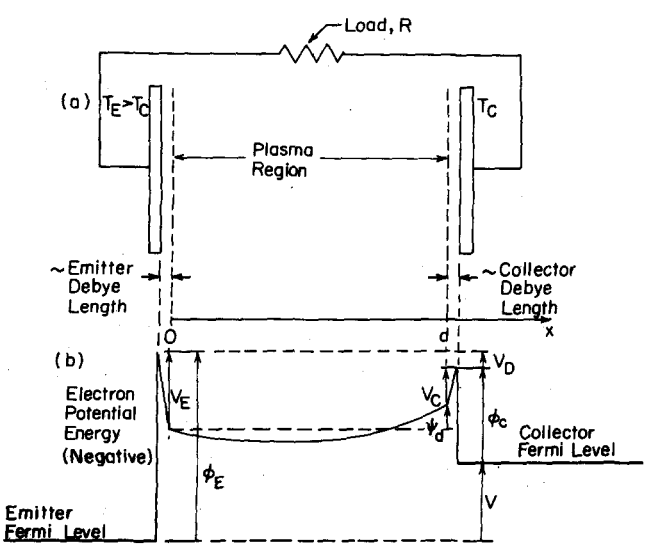

FIG. 1. (a) Schematic diagram of a thermionic diode. (b) Motive diagram assumed in this study.

negligible width. The plasma is one dimensional, of low energy, and consists of ions, electrons, and neutral atoms. The electron potential energy is due entirely to the electric field and varies in the general manner given by the motive diagram in Fig. 1(b). Here, the emitter sheath, of height V_E, is accelerating; the collector sheath, of height V_C, is retarding; and no assumption is made regarding the form of the electrical potential in the plasma. The terms "accelerating" and "retarding" refer to sheaths that accelerate or retard electrons as they move toward the collector. The emitter and collector work functions are given by ϕ_E and ϕ_C, respectively; the arc drop is denoted by V_D and the output voltage by V. Position x varies from zero at the emitter, where the electron potential ψ is set equal to zero, to d at the collector, where the electron potential is ψ_d.

For low degrees of ionization,

$$n_e = n_i \ll n_n, \tag{1}$$

where n_α is the concentration of species α. The subscripts e, i, and n, indicate electrons, ions, and neutral atoms, respectively.

Assuming collisional coupling between heavy particle species, we have

$$\theta_i = \theta_n, \tag{2}$$

where $\theta_\alpha = kT_\alpha$ is the temperature of species α in energy units.

B. Governing equations

For the assumed type of plasma, the equation of state is

$$p = n_e(\theta_e + \theta_n) + n_n\theta_n \approx n_n\theta_n, \tag{3}$$

where p is the total pressure, and the transport equations, which are derived using those of Wilkins and Gyftopoulos,[1] are

$$\frac{d\Gamma_e}{dx} = \frac{d\Gamma_i}{dx} = S, \tag{4}$$

$$\frac{\Gamma_e}{\mu_e} = -\frac{dp_e}{dx} - n_e\frac{d\psi}{dx}, \tag{5}$$

$$\frac{\Gamma_i}{\mu_i} = -\frac{dp_i}{dx} + n_e\frac{d\psi}{dx}, \tag{6}$$

$$Q_e = \Gamma_e(\tfrac{5}{2}\theta_e + \psi) - 2n_e\mu_e\theta_e\frac{d\theta_e}{dx}, \tag{7}$$

$$Q_n = -2n_n\mu_n\theta_n\frac{d\theta_n}{dx}, \tag{8}$$

where S is the ionization rate density, and, for species α, Γ_α is the particle flux, μ_α is the mobility, Q_α is the energy flux, and $p_\alpha = n_\alpha\theta_\alpha$ is the pressure.

The mobilities are given by

$$\mu_e^{-1} = m_e\bar{c}_e(\sigma_{en}n_n + \sigma_{ei}n_e), \tag{9}$$

$$\mu_i^{-1} = \sqrt{2}\, m_n\bar{c}_n\sigma_{in}n_n, \tag{10}$$

$$\mu_n^{-1} = \sqrt{2}\, m_n\bar{c}_n\sigma_{nn}n_n, \tag{11}$$

where m_α is the mass of species α, $\sigma_{\alpha\beta}$ is the collision cross section for species α and β, and

$$\bar{c}_\alpha = (8\theta_\alpha/\pi m_\alpha)^{1/2} \tag{12}$$

is the mean thermal speed of species α. Note that, in using these equations, we assume that (i) charged particles are created in electronion pairs, (ii) thermal diffusion and the transfer of directed momentum from electrons to ions may be neglected, and (iii) the energy flux carried by ions is negligible with respect to that carried by neutrals.

Making the additional assumption that radiation losses and energy transfer from electrons to heavy particles are small gives us

$$\frac{dQ_n}{dx} = 0, \tag{13}$$

$$\frac{dQ_e}{dx} = -V_iS, \tag{14}$$

where V_i is the ionization potential.

For collisonal ionization and three-body recombination, the net ionization rate is given by[4]

$$S = \beta_r n_e(n_s^2 - n_e^2), \tag{15}$$

where we have employed the principle of detailed balancing,

$$\beta_r\,(\mathrm{cm}^6/\mathrm{sec}) \approx 4\times10^{-27}[\theta_e\,(\mathrm{eV})]^{-9/2} \tag{16}$$

is the three-body recombination rate constant, and

$$n_s = n_n^{1/2}(m_e\theta_e/2\pi\hbar^2)^{3/4}\exp(-V_i/2\theta_e) \tag{17}$$

is the Saha electron concentration. To derive Eq. (16), we utilize the temperature dependence determined by Mansbach and Keck[5] and choose a value of the coefficient which gives the best possible agreement with experiments[6–11] after the empirical values are corrected for radiative cascading. In the vicinity of a reference temperature θ^*, a good approximation for n_s is

$$n_s = n^*\exp(-V^*/\theta_e), \tag{18}$$

where

$$n^* = n_n^{1/2}(2.72m_e\theta^*/2\pi\hbar^2)^{3/4}, \tag{19}$$

$$V^* = \tfrac{1}{2}V_i + \tfrac{3}{4}\theta^*. \tag{20}$$

C. Boundary conditions

The emitter boundary conditions that were used are

$$\Gamma_{e0} = \Gamma_E - R_{e0}\exp(-V_E/\theta_{e0}), \tag{21}$$

$$\Gamma_{i0} = -2R_{i0}, \tag{22}$$

$$Q_{e0} = \Gamma_E(2\theta_E + V_E) - (\Gamma_E - \Gamma_{e0})(2\theta_{e0} + V_E), \tag{23}$$

and the collector boundary conditions used are

$$\Gamma_{ed} = R_{ed}\exp(-V_C/\theta_{ed}), \tag{24}$$

$$\Gamma_{id} = 2R_{id}, \tag{25}$$

$$Q_{ed} = \Gamma_{ed}(2\theta_{ed} + V_C + \psi_d), \tag{26}$$

where Γ_E is the emitter saturation current,

$$R_\alpha = \tfrac{1}{4}n_\alpha\bar{c}, \tag{27}$$

is the random current for species α, and the subscripts 0 and d indicate evaluation at the emitter or collector end of the plasma, respectively. These boundary conditions are a variation of those used by McCandless *et al.*[2] At the time this work was undertaken, no rigor-

ously derived set of boundary conditions was available. However, Keck[12] has recently developed a set of boundary conditions using the Krook approximation to the Boltzmann equation. These boundary conditions have not, as yet, been used in an analysis of a converter. We can, however, easily determine under what circumstances the boundary conditions used here are equivalent to the correct ones. We find that if $(\lambda_{in}/2\theta_e)\,d\psi/dx$ is not greater than of order unity, where λ_{in} is the ion-neutral mean free path, and if R_e and $(d/T_e)dT_e/dx$ at both electrodes are not much greater than unity, then the two sets of boundary conditions are equivalent when

$$1 \lesssim V_E/\theta_{e0} \lesssim 5, \tag{28}$$

$$1 \lesssim V_C/\theta_{ed} \lesssim 5. \tag{29}$$

III. METHOD OF SOLUTION

A. Temperature distribution of neutrals

To obtain the temperature distribution of the neutral atoms, we substitute (11) and (12) into (8) and integrate for constant σ_{nn}. Then for temperatures of neutrals at the plasma boundaries equal to the corresponding electrode temperatures, we obtain

$$\theta_n = \theta_E[1 - \eta(1 - \epsilon_{CE})^{3/2}]^{2/3}, \tag{30}$$

where

$$\eta = x/d \tag{31}$$

is a dimensionless distance and

$$\epsilon_{CE} = \theta_C/\theta_E \tag{32}$$

is the ratio of the collector temperature θ_C to the emitter temperature θ_E.

B. Electron density distribution

In order to make the integration of the ionization rate S tractable, we assume that S, given by (15), can be approximated by the function

$$S^* = A \tanh\left(\frac{\eta + a}{b}\right) \sec^2\left(\frac{\eta + a}{b}\right), \tag{33}$$

where A, a, and b are parameters which are to be adjusted so as to give the best fit of S and S^*. This function gives a good approximation to the variation of the electron production with position which has been obtained in previous studies.[13–15] Justification of the assumed form for any particular case, however, can be obtained only after S has been calculated and compared with S^*. As will be seen, this form is applicable to converters with small values of pd in which nonequilibrium conditions exist.

Substituting S^* for S in Eq. (4), integrating, and applying the condition $\Gamma_i = \Gamma_{id}$ at the collector, we obtain

$$\Gamma_i = \Gamma_e - J/e$$
$$= \Gamma_{id} + \tfrac{1}{2}Abd(\tanh^2\delta - \tanh^2\delta_d), \tag{34}$$

where J is the net negative charge flux, e is the unit charge,

$$\delta = (\eta + a)/b \tag{35}$$

is a nondimensional measure of position, and $\delta_d = (1 + a)/b$ is the value of δ at the collector.

Adding (5) and (6), and using (9), (10), (12), (25), (27), and (31), and assuming $\Gamma_e \approx \Gamma_{ed}$ gives us

$$\frac{d\bar{P}}{d\eta} + \frac{d_{ei}}{\bar{R}_{ed}}\bar{P} = -d_{in}\left(\bar{\Gamma}_i + \frac{\epsilon_{ei}}{\bar{R}_{ed}}\right), \tag{36}$$

where

$$\bar{P} = n_e(\theta_e + \theta_i)/n_{ed}(\theta_{ed} + \theta_C), \tag{37}$$

$$\bar{\Gamma}_i = \Gamma_i/\Gamma_{id}, \tag{38}$$

$$d_{ei} = n_{ed}\sigma_{ei}\,d[2(\theta_e\theta_{ed})^{1/2}/\pi(\theta_{ed} + \theta_i)], \tag{39}$$

$$d_{in} = n_n\sigma_{in}\,d[4(2\theta_i\theta_C)^{1/2}/\pi(\theta_{ed} + \theta_C)], \tag{40}$$

$$\epsilon_{ei} = (\sigma_{en}/\sigma_{in})[\theta_e\theta_{ed}/8\theta_i\theta_C]^{1/2}, \tag{41}$$

$$\bar{R}_e = R_e/\Gamma_e. \tag{42}$$

Since the ions carry only a small fraction of the total particle flux, which is constant, across the converter, the approximation $\Gamma_e \approx \Gamma_{ed}$ is a good one.

The terms in brackets in (39)—(41) are all of order unity. Therefore d_{ei} and d_{in} are essentially the converter spacing measured in electron-ion and ion-neutral mean free paths, respectively, and ϵ_{ei} is essentially the ratio of the ion-neutral to the electron-neutral mean free path. Since the temperature dependence of the cross sections is weak and the concentration of neutrals is nearly constant, we may treat d_{ei}, d_{in}, and ϵ_{ei} as constants (to be evaluated at the maximum point of S^*).

At this point we investigate the relative orders of magnitude of the terms $d_{ei}\bar{P}/\bar{R}_{ed}$ and $d_{in}\epsilon_{ei}/\bar{R}_{ed}$ in (36). The first of these quantities divided by the second is $\sigma_{ei}n_i/\sigma_{en}n_n$. Using the cross sections given in Table I,[16] we find that this ratio reduces to $25n_i/n_n$, which, for most converters of interest is much less than unity. Therefore, the term $d_{ei}\bar{P}$ may be neglected in (36).

Integration of (36) with the condition $\bar{P} = 1$ at $\eta = 1$ then gives us

$$\bar{P} = 1 + \bar{d}\{[1 + B\,\mathrm{sech}^2\delta_d][(1 - \eta)/(1 + a)]$$
$$- (B/\delta_d)[\tanh\delta_d - \tanh\delta]\}, \tag{43}$$

where

$$\bar{d} = (1 + a)(1 + \epsilon_{ei}/\bar{R}_{ed})d_{in}, \tag{44}$$

$$B = Abd/2\Gamma_{id}(1 + \epsilon_{ei}/\bar{R}_{ed}). \tag{45}$$

We expect that $a \ll 1$. From the assumption that the temperatures are all of the same order of magnitude and that $\bar{R}_{ed}$ is not small compared to unity, we find that $\epsilon_{ei}/\bar{R}_{ed} \ll 1$. Thus, $\bar{d}$ is essentially the same as d_{in}. To obtain an expression for the electron production in terms of $\bar{P}$, we substitute (37) into (15) and use (25) and (27). This gives us

$$S = (2\Gamma_{id}/d)d_r\bar{P}(\bar{P}_s^2 - \bar{P}^2), \tag{46}$$

TABLE I. Values of collision cross sections (from Ref. 16).

σ_{in}	≈ 1200 Å^2
σ_{en}	≈ 400 Å^2
σ_{nn}	≈ 100 Å^2
σ_{ei}	$\sim 10^4$ Å^2

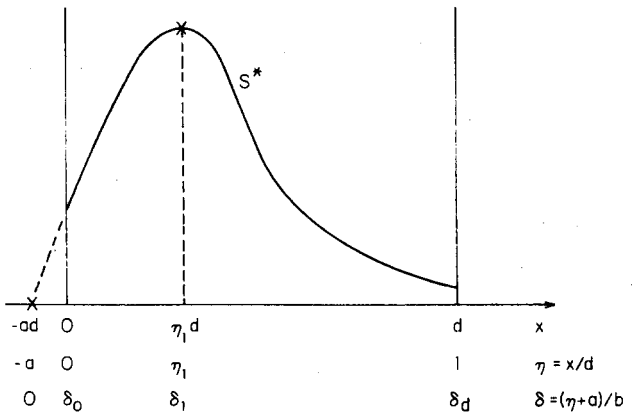

FIG. 2. Assumed form of ionization rate S^*, given by (33). Points where S^* is matched with S are indicated by ×.

where

$$\bar{P}_s = n_s(\theta_e+\theta_i)/n_{ed}(\theta_{ed}+\theta_C), \tag{47}$$

$$d_r = \left(\frac{\beta_r n_{ed}^2 d}{\bar{c}_{id}}\right)\left(\frac{\theta_{ed}+\theta_C}{\theta_e+\theta_i}\right)^3. \tag{48}$$

Note that $[(\theta_{ed}+\theta_C)/(\theta_e+\theta_i)]^3 \sim 1$, and from (15) the mean time for recombination is $(\beta_r n_e^2)^{-1}$. Therefore d_r is essentially the converter spacing divided by the mean free path for ion recombination at the collector.

We now determine values of the parameters B, a, and b which will give the best fit of S^* to S. Figure 2 shows the form of the function S^* given by (33). Note that, in this figure, $\delta_0 = a/b$ is the value of δ at the emitter, and η_1 and δ_1 are the values of η and δ, respectively, at the point of maximum electron production. We anticipate that by matching at the point of maximum electron production, where $\eta = \eta_1$, and at the extrapolated end point, where $\eta = -a$, a good over-all fit of S and S^* will be obtained.

First we match S and S^* at the extrapolated end point. Using (33), (37), (46), and the condition $(S)_{\eta=-a} = (S^*)_{\eta=-a} = 0$, we have

$$1 + \bar{d}[1 + B\,\mathrm{sech}^2\delta_d - (B/\delta_d)\tanh\delta_d] = 0. \tag{49}$$

Matching at the position of maximum electron production we use $(dS/d\eta)_1 = (dS^*/d\eta)_1 = 0$ to obtain

$$\left((\bar{P}_s^2 - 3\bar{P}^2)\frac{d\bar{P}}{d\eta} + 2\bar{P}\bar{P}_s\frac{d\bar{P}_s}{d\eta}\right)_1 = 0, \tag{50}$$

$$\delta_1 = \coth^{-1}\sqrt{3} \approx 0.66, \tag{51}$$

where the subscript 1 denotes evaluation at $\eta = \eta_1$. It should be noted that, in the differentiation of S, the variation of d_r is considered to be negligible. Finally, (45) and the condition $S_1 = S_1^*$ yield

$$2B(1+\epsilon_{ei}/\bar{R}_{ed})/3\sqrt{3}\,b = d_{r1}\bar{P}_1(\bar{P}_{s1}^2 - \bar{P}_1^2). \tag{52}$$

Equations (49)—(52) are sufficient to determine B, a, and b. We now derive some additional relationships which will be required.

Evaluating (34) at the emitter, using the boundary conditions (22) and (25) as well as the equations (12), (27), (32), (37), and (38), we get

$$\bar{\Gamma}_{i0} = -\bar{P}_0[(\theta_{ed}+\theta_C)/(\theta_{e0}+\theta_E)](\epsilon_{CE})^{1/2}$$
$$= 1 + B(1+\epsilon_{ei}/\bar{R}_{ed})(\tanh^2\delta_0 - \tanh^2\delta_d). \tag{53}$$

From (12), (25), and (27) we obtain

$$\Gamma_{e0} = \Gamma_{e0}/\Gamma_{ed} = 1 - \epsilon_m\bar{R}_{ed}(1-\bar{\Gamma}_{i0}), \tag{54}$$

where, for $T_C \approx 620°\mathrm{K}$ and $T_{ed} \approx 2600°\mathrm{K}$,

$$\epsilon_m = \left(\frac{\Gamma_{id}}{\Gamma_{ed}}\right)/\bar{R}_{ed} = 2\left(\frac{m_e\theta_C}{m_n\theta_{ed}}\right)^{1/2} \approx \frac{1}{500}. \tag{55}$$

Combining (12), (22), (25), (27), (32), (38), and (42) gives us

$$\bar{R}_{e0} = \frac{R_{e0}}{\Gamma_{e0}} = -\bar{\Gamma}_{i0}\epsilon_{CE}^{1/2}\left(\frac{\theta_{e0}}{\theta_{ed}}\right)^{1/2}\bar{R}_{ed}/\bar{\Gamma}_{e0}. \tag{56}$$

From (43) and (49) we have

$$B = (\bar{d}+1)\delta_d\coth\delta_d/\bar{d}(1-C), \tag{57}$$

$$\bar{P} = (\bar{d}/\delta_d)(B\tanh\delta - D\delta), \tag{58}$$

where

$$C = 2\delta_d/\sinh 2\delta_d, \tag{59}$$

$$D = 1 + B\,\mathrm{sech}^2\delta_d$$
$$= (\bar{d}+C)/\bar{d}(1-C). \tag{60}$$

Combining (44), (51), (52), and (57)—(60), we obtain

$$\left(\frac{\bar{P}_s}{\bar{P}}\right)_1^2 = 1 + \frac{2E^2}{\epsilon_r\bar{d}^2(\bar{d}+1)^2}, \tag{61}$$

where

$$E = \frac{(1-C)\delta_d}{\coth\delta_d}\left(1 - 1.14\frac{D}{B}\right)^{-3/2} \tag{62}$$

and

$$\epsilon_r = d_{r1}/d_{in}(1+\epsilon_{ei}/\bar{R}_{ed})^2$$
$$= \frac{\pi}{4\sqrt{2}}\frac{(m_n/m_e)^{1/2}}{(1+\epsilon_{ei}/\bar{R}_{ed})^2}\left(\frac{\beta_{r1}n_{ed}}{\sigma_{in}\bar{c}_{ed}}\right)\left(\frac{n_{ed}(\theta_i\theta_{ed})^{1/2}}{p}\right)$$
$$\times\left(\frac{\theta_{ed}+\theta_C}{\theta_{e1}+\theta_{i1}}\right)^3\left(\frac{\theta_{ed}+\theta_C}{\theta_C}\right). \tag{63}$$

Since $\epsilon_{ei}/\bar{R}_{ed} \ll 1$, ϵ_r is essentially the ratio of the ion-neutral mean free path to the mean free path for ion recombination at the point of maximum electron production.

Substituting (61) into (50) gives us

$$\Delta\chi_1 \equiv -\left(\frac{d\ln\bar{P}_s}{d\eta}\right)_1$$
$$= \left(\frac{E^2 - \epsilon_r\bar{d}^2(\bar{d}+1)^2}{E^2 + \frac{1}{2}\epsilon_r\bar{d}^2(\bar{d}+1)^2}\right)F, \tag{64}$$

where

$$F = \tfrac{1}{2}\left(\frac{d\ln\bar{P}}{d\eta}\right)_1$$
$$= \frac{\delta_d - 3(\bar{d}+C)/2(\bar{d}+1)\coth\delta_d}{\sqrt{3}\,(1+a)(1-1.14D/B)}. \tag{65}$$

We observe that, when $\epsilon_r\bar{d}^2(\bar{d}+1)^2 \ll E^2$, (64) reduces to $\Delta\chi_1 = F$. When this is the case, $\Delta\chi_1$ becomes independent of J, since the dependence of $\Delta\chi_1$ on J is contained entirely in ϵ_r. We expect that $a \ll 1$ so that F is a function of $\bar{d}$ and δ_d only. From (49), (57), and (59), we see

that δ_d is a function of $\bar{d}$ only. Thus F can be expressed as a function of $\bar{d}$ only. It can be shown that many of the variables will, for this special case, either be independent of J or will depend on it in some simple manner. It can readily be proven that E cannot take on a value smaller than approximately 5.4. Therefore $\Delta\chi_1$ will be independent of J when $\epsilon_r \bar{d}^2(\bar{d}+1)^2 \ll (5.4)^2$.

We expect that, for most conditions of interest, $(\delta_0 \coth\delta_0 - 1) \ll (\delta_d \coth\delta_d - 1)$ so that, by substituting (57) and (60) into (58) and evaluating $\bar{P}$ at $\eta = 0$, we obtain

$$\bar{P}_0 \approx (\bar{d}/\delta_d)(B - D)\tanh\delta_0. \tag{66}$$

Combining (65) and (37) and substituting into (53) gives us

$$B(1 + \epsilon_{ei}/\bar{R}_{ed})\tanh^2\delta_0 + G\tanh\delta_0 - H = 0. \tag{67}$$

Solving this equation for $\tanh\delta_0$ and neglecting the negative root, we have

$$\tanh\delta_0 = \frac{G}{2B(1 + \epsilon_{ei}/\bar{R}_{ed})}\left\{\left[1 + \frac{4BH}{G^2}\left(1 + \frac{\epsilon_{ei}}{\bar{R}_{ed}}\right)^{1/2}\right] - 1\right\}, \tag{68}$$

where

$$G = \frac{\bar{d}(B - D)}{\delta_d(\epsilon_{CE})^{1/2}}\left(\frac{\theta_{ed} + \theta_C}{\theta_{e0} + \theta_E}\right), \tag{69}$$

$$H = B(1 + \epsilon_{ei}/\bar{R}_{ed})\tanh^2\delta_d - 1. \tag{70}$$

C. Electron potential energy

By combining (5) and the relation $p_i = p_e\theta_i/\theta_e$ to eliminate dp_i/dx from (6), and then using (3), (9), (10), (12), (25), (27), (31), (35), (37), (38), (40), (41), and the approximations $\mu_i \ll \mu_e$ and $\Gamma_e \approx \Gamma_{ed}$, we obtain

$$\frac{d\psi}{d\eta} = \frac{d_{in}}{\bar{P}}\left(\bar{\Gamma}_i\theta_e - \frac{\epsilon_{ei}}{\bar{R}_{ed}}\theta_i\right) + \theta_e\frac{d}{d\eta}\ln\left(1 + \frac{\theta_i}{\theta_e}\right) - \frac{d_{ei}}{\bar{R}_{ed}}\theta_i. \tag{71}$$

Substituting (44), (45), and (70) into (34) gives us

$$\bar{\Gamma}_i = -H + B(1 + \epsilon_{ei}/\bar{R}_{ed})\tanh^2\delta. \tag{72}$$

Substituting (58) and (72) into (71) and integrating, we get

$$\psi = \psi_1 + \psi_2 + \psi_3 + \psi_4, \tag{73}$$

where

$$\psi_1 = \int_0^\eta \theta_e\left[\frac{d}{d\eta'}\ln\left(1 + \frac{\theta_i}{\theta_e}\right)\right]d\eta', \tag{74}$$

$$\psi_2 = \int_{\delta_0}^{\delta} \frac{[\theta_e I - (\epsilon_{ei}/\bar{R}_{ed})\theta_i]\tanh^2\delta'}{(1 + \epsilon_{ei}/\bar{R}_{ed})(B\tanh\delta' - D\delta')}d\delta', \tag{75}$$

$$\psi_3 = -\int_{\delta_0}^{\delta} \frac{[\theta_e H + (\epsilon_{ei}/\bar{R}_{ed})\theta_i]\mathrm{sech}^2\delta'}{(1 + \epsilon_{ei}/\bar{R}_{ed})(B\tanh\delta' - D\delta')}d\delta', \tag{76}$$

$$\psi_4 = -(d_{ei}/\bar{R}_{ed})\int_0^\eta \theta_i\, d\eta', \tag{77}$$

where

$$I = B(1 + \epsilon_{ei}/\bar{R}_{ed})\mathrm{sech}^2\delta_d + 1. \tag{78}$$

To determine ψ_1, we note that θ_e varies slowly across the converter and obtain

$$\psi_1 \approx \theta_i - \theta_E. \tag{79}$$

In evaluating ψ_2, we note that the integrand increases rapidly with δ so that the value of the integral is determined mainly by the contribution from the vicinity of the upper limit. Therefore,

$$\psi_2 \approx \frac{[\theta_e I - (\epsilon_{ei}/\bar{R}_{ed})\theta_i]\tanh^2\delta}{1 + \epsilon_{ei}/\bar{R}_{ed}}\int_{\delta_0}^{\delta}\frac{1}{B\tanh\delta - D\delta'}d\delta'$$

$$= \frac{[\theta_e I - (\epsilon_{ei}/\bar{R}_{ed})\theta_i]\tanh^2\delta}{[1 + \epsilon_{ei}/\bar{R}_{ed}]D}\ln\left(\frac{\tanh\delta - (D/B)\delta_0}{\tanh\delta - (D/B)\delta}\right). \tag{80}$$

Similarly, since, in the case of ψ_3, the integrand decreases rapidly with increasing δ, it is a good approximation to set $\tanh\delta = \delta$ and $\theta_e H + \epsilon_{ei}/\bar{R}_{ed}\theta_i = \theta_{e0}H + \epsilon_{ei}/\bar{R}_{ed}\theta_E$ for the integration. This gives us

$$\psi_3 \approx -\frac{\theta_{e0}H + (\epsilon_{ei}/\bar{R}_{ed})\theta_E}{(1 + \epsilon_{ei}/\bar{R}_{ed})(B - D)}\ln\frac{\tanh\delta}{\tanh\delta_0}. \tag{81}$$

Substituting (30) into (77), we easily obtain

$$\psi_4 = -\frac{3}{5(1 - \epsilon_{CE}^{3/2})}\frac{d_{ei}}{\bar{R}_{ed}}\theta_E\left[1 - \left(\frac{\theta_i}{\theta_E}\right)^{5/2}\right]. \tag{82}$$

We note that (80) and (81) become increasingly better approximations as δ/δ_0 increases. In particular, a fairly good value for the electron potential at the collector will be obtained.

Now we find from (21), (24), (42), and Fig. 1 that the sheath heights and the arc drop are given by

$$V_C = \theta_{ed}\ln\bar{R}_{ed}, \tag{83}$$

$$V_E = \theta_{e0}\ln\left(\frac{\bar{R}_{e0}}{\Gamma_E/\Gamma_{e0} - 1}\right), \tag{84}$$

and

$$V_D = V_E - V_C - \psi_d. \tag{85}$$

Another relation for the arc drop can be obtained by integrating (4) and (14), combining the results with (23) and (26), and using (85). This gives us

$$V_D = 2(\Gamma_E/\Gamma_{ed})(\theta_{e0} - \theta_E) - 2(\theta_{e0} - \theta_{ed}) + \epsilon_m\bar{R}_{ed}(1 - \bar{\Gamma}_{i0})(V_i + 2\theta_{e0} + V_E). \tag{86}$$

If, instead of a monotonically varying sheath at the emitter, there exists a double-valued sheath, a correction must be made to the relationship for the arc drop. In Fig. 3 we see the form taken by the motive diagram when there is a double sheath at the emitter. The subscript M indicates evaluation at conditions corresponding to the largest value of the saturation current J_E at which there is a double sheath. Thus,

$$\Delta V_E \equiv V_E - V_{EM} = V_D - V_{DM}. \tag{87}$$

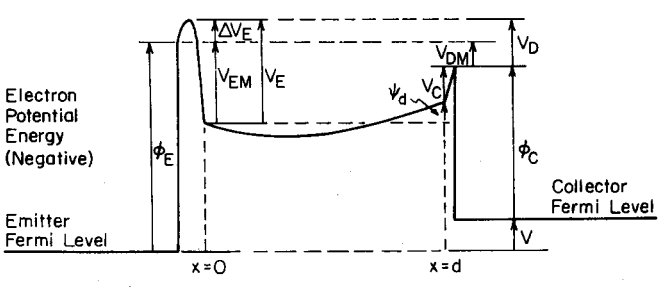

FIG. 3. Motive diagram when there is a double sheath at the emitter.

Assuming a Boltzmann distribution at the emitter sheath at the temperature of the emitter, we have for constant J,

$$V_{DM} = V_D + \theta_E \ln(J_{EM}/J_E), \tag{88}$$

where J_{EM} is the minimum value of J_E at which a double sheath exists. To determine J_{EM}, a theory of the Debye sheaths in a thermionic converter is required. To our knowledge, no adequate theory exists and J_{EM} is unknown at present.

D. Electron temperature

Using (3), (9), (10), (12), (25), (27), (31), (37), (39), (40), (41) and the approximation $\Gamma_e \approx \Gamma_{ed}$, we write (7) in the form

$$\frac{d\theta_e}{d\eta} - \tfrac{5}{4}\rho\theta_e = -\tfrac{1}{2}\rho\left(\frac{Q_e}{\Gamma_e} - \psi\right), \tag{89}$$

where

$$\rho = \left(1 + \frac{\theta_i}{\theta_e}\right)\left(\frac{\epsilon_{ei}}{\bar{R}_{ed}}\frac{d_{in}}{\bar{P}} + d_{ei}\right). \tag{90}$$

Integration of (89) yields

$$\theta_e \exp(-\tfrac{5}{4}K) - \theta_{e0} = -\frac{1}{2}\int_0^\eta \exp(-\tfrac{5}{4}K)\left(\frac{Q_e}{\Gamma_e} - \psi\right)\rho\, d\eta', \tag{91}$$

where

$$K = \int_0^\eta \rho\, d\eta'. \tag{92}$$

Since, from (14) and (73), $Q_e = Q_{e0} - V_i(\Gamma_i - \Gamma_{i0})d$, and since we have relations for ψ, (91) can be integrated numerically to give us a relation of the form $f\{\theta_{e0}, \theta_{ed}, \delta_d, \bar{R}_{ed}\} = 0$. In practice, however, this makes the solution difficult. We therefore, as a first approximation, instead assume that $(Q_e/\Gamma_e - \psi)$ may be considered to be constant. Integration of (91) then gives us

$$\theta_e = \theta_{ed} + (\theta_{e0} - \theta_{ed})\{1 - \exp[-\tfrac{5}{4}(K_d - K)]\}[1 - \exp(-\tfrac{5}{4}K)\, d]^{-1}. \tag{93}$$

From (26), (83), (89), and (93), we obtain

$$\bar{\theta}_{e0} = \theta_{e0}/\theta_{ed} = 1 - \tfrac{1}{5}(1 - 2\ln\bar{R}_{ed})[1 - \exp(-\tfrac{5}{4}K_d)]. \tag{94}$$

The variation of ρ is due primarily to the variation of $\bar{P}$. We therefore obtain from (92),

$$K = \ln\left[\left(\frac{\tanh\delta}{\tanh\delta_0}\right)^{\alpha_1}\left(\frac{B\tanh\delta - D\delta_0}{B\tanh\delta - D\delta}\right)^{\alpha_2}\right] + \frac{d_{ei}}{\bar{R}_{ed}}\left(1 + \frac{\theta_c}{\theta_{ed}}\right)\left(\frac{\delta - \delta_0}{\delta_d - \delta_0}\right), \tag{95}$$

where

$$\alpha_1 = \frac{\epsilon_{ei}}{\bar{R}_{ed}}\frac{1 + \theta_C/\theta_{ed}}{(1 + \epsilon_{ei}/\bar{R}_{ed})(B - D)}, \tag{96}$$

$$\alpha_2 = \frac{\epsilon_{ei}}{\bar{R}_{ed}}\frac{(1 + \theta_C/\theta_{ed})\tanh^2\delta}{(1 + \epsilon_{ei}/\bar{R}_{ed})D}. \tag{97}$$

From (18), (47), (64), (92), and (93) we have

$$\Delta\chi_1 = \tfrac{5}{4}\rho_1\left(\frac{V^*}{\theta_{e1}}\right)\left(\frac{\theta_{e0} - \theta_{ed}}{\theta_{e1}}\right)\{\exp[\tfrac{5}{4}(K_d - K_1)] - 1\}^{-1}. \tag{98}$$

IV. NUMERICAL METHODS

A. Equations to be solved

To obtain a numerical solution, we formulate the problem as one of solving a system of three simultaneous transcendental equations for the unknowns θ_{e1}, δ_d, and $\bar{R}_{ed}$. Two of the equations are of the functional forms

$$f_1\{\theta_{e1}, \delta_d, \bar{R}_{ed}\} = 0, \tag{99}$$

$$\theta_{e1} = f_2\{\theta_{e1}, \delta_d, \bar{R}_{ed}\}, \tag{100}$$

and for the third, we have a choice of either

$$\delta_d = f_3\{\theta_{e1}, \delta_d, \bar{R}_{ed}\} \tag{101}$$

or

$$\bar{R}_{ed} = f_4\{\theta_{e1}, \delta_d, \bar{R}_{ed}\}. \tag{102}$$

In the routine employed, three separate equations are used which, together, are equivalent to (102).

B. Methods of solution

To provide a motivation for the methods used and to obtain an understanding of the nature of the solutions which will be obtained, we first rewrite and then sketch (64). Equation (64) can be written in the form

$$\bar{R}_{ed}\phi = E\left(\frac{F - \Delta\chi_1}{F + \frac{1}{2}\Delta\chi_1}\right)^{1/2}, \tag{103}$$

where

$$\phi = \epsilon_r^{1/2}\bar{d}(\bar{d} + 1)/\bar{R}_{ed}. \tag{104}$$

In Fig. 4 we have a contour plot of (103). From inspection of this figure we conclude that under nonequilibrium conditions ($\bar{R}_{ed}\phi \ll 5.4$) there is only one solution to be found for a given value of $\bar{R}_{ed}\phi$. This is due to the fact that in a nonequilibrium situation, the electron production S has only one extremum to which the maximum in the assumed form, S^*, can be matched so that (50), and therefore also (64), has only one solution. When the plasma is in local thermodynamic equilibrium ($\bar{R}_{ed} \gg$

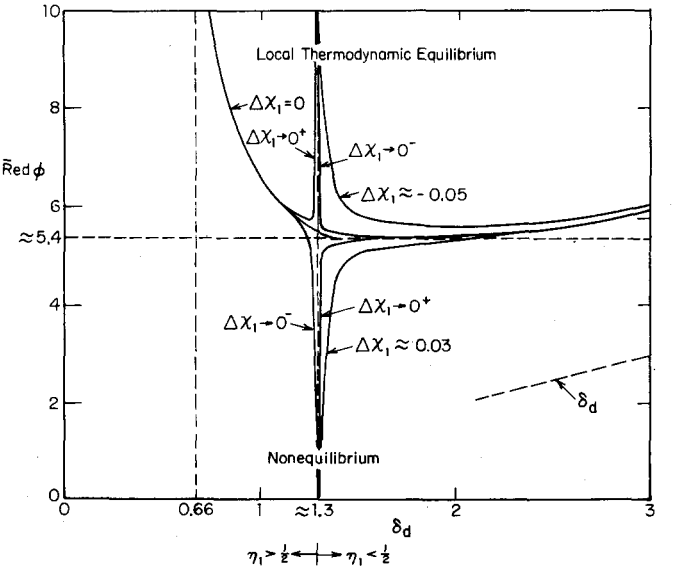

FIG. 4. Contour plot of Eq. (103).

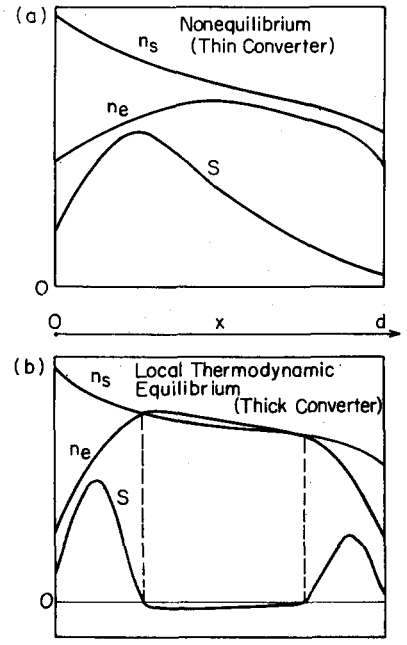

FIG. 5. (a) Conditions existing in a nonequilibrium situation (corresponding to bottom of Fig. 4 where $\bar{R}_{ed}\phi \lesssim 5.4$). (b) Conditions existing when equilibrium is approached along most of the interelectrode gap (corresponding to $\bar{R}_{ed}\phi \gg 5.4$).

5.4), however, S contains two maxima and therefore three extrema to which the maximum in S^* may be matched. Thus, a form of S^* which contains two maxima would be required to obtain accurate equilibrium solutions.

That these results are in agreement with what we would expect physically becomes clear from Fig. 5. In the nonequilibrium situation, the converter is not sufficiently thick for the electrons to achieve an equilibrium concentration before they reach the collector; S, then, achieves a maximum near the emitter and decreases in magnitude as n_e approaches n_s. In the thick converter case, on the other hand, n_e becomes as large as n_s at some point in the converter, overshoots slightly, and becomes smaller than n_s in the vicinity of the collector. Maxima in S will then exist in the two regions where n_e is smaller than n_s.

Since, from (35), (51), and the assumption that $\delta_0 \ll \delta_1$,

$$\eta_1 = (\delta_1 - \delta_0)/(\delta_d - \delta_0) \approx 0.66/\delta_d, \tag{105}$$

the maximum in the electron production will be near the emitter ($\eta_1 < \frac{1}{2}$) for $\delta_d > 1.3$ and near the collector ($\eta_1 > \frac{1}{2}$) for $\delta_d < 1.3$. Since the variation of $\bar{P}_S$ is due primarily to that of n_s, we have, from (18), (47), and (64),

$$\Delta\chi_1 = \frac{-V^*}{\theta_{e1}^2}\frac{d\theta_e}{d\eta}\bigg|_1.$$

Therefore, for monotonically varying electron temperature across the converter, the sign of $(\bar{\theta}_{e0} - 1)$, given by (94), must be the same as that of $\Delta\chi_1$. For many cases of interest [see (95)–(97)] $\exp(-\frac{5}{4}Kd) \ll 1$. It can easily be seen from (94) that when this is so

$$(\bar{\theta}_{e0} - 1)/(\bar{R}_{ed} - 1.65) > 0. \tag{106}$$

To obtain an approximate relation for ϕ, we use the reference values $T_e = 2800\,^\circ\mathrm{K}$, $V^* = 8T_e$, $T_E = 1800\,^\circ\mathrm{K}$, $T_C = 620\,^\circ\mathrm{K}$ with $T_{i1} = (T_E T_C)^{1/2}$, and the assumptions $\epsilon_{ei}/\bar{R}_{ed} \ll 1$ and $a \ll 1$. Then using (12), (16), (44), and Table I, (104) reduces to

$$\phi \approx 2.5\times10^{-4}\frac{J(\mathrm{A/cm^2})d_{in}(d_{in}+1)}{[p(\mathrm{Torr})]^{1/2}}. \tag{107}$$

Figure 4, in conjunction with (106) and (107), can be used to predict where solutions will be found.

To obtain solutions, we specify the values of p, $\bar{d}$, T_E, T_C, J, J_E, m_e, m_n, σ_{in}, σ_{en}, σ_{nn}, and V_i. Then what is essentially a scan along δ_d and/or a scan along $\bar{R}_{ed}$ is performed. In Fig. 4 we see that for small values of $\bar{R}_{ed}$, corresponding to nonequilibrium conditions, the branches on which solutions are to be sought are nearly vertical. The value of ϕ will not vary very much. We therefore expect scans along $\bar{R}_{ed}$ to be most likely to yield solutions. By similar reasoning, it is anticipated that scans along δ_d will be most profitable in searches for solutions on the near-horizontal sections. Note that, as δ_d becomes large, $\bar{R}_{ed}\phi$ asymptotically approaches δ_d.

In the scans along δ_d, it is required that (99), (100), and (102) be satisfied, and, in scans along $\bar{R}_{ed}$, (101) must be satisfied instead of (102). In order to start the scans, guesses must be made as to the values of some of the variables. At a value of the scan parameters for which (99) is satisfied, these variables are evaluated and the values obtained are used to start another scan. This procedure is repeated until convergence is achieved.

V. RESULTS AND DISCUSSION

A. Some illustrative solutions (Ref. 17)

Solutions were obtained for a cesium-filled converter at an emitter temperature T_E of 1800°K, a collector tem-

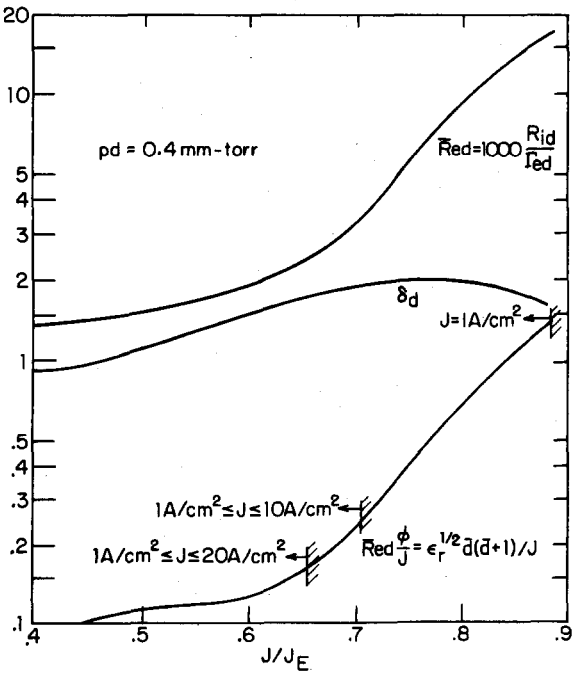

FIG. 6. $\bar{R}_{ed}$, $R_{ed}\phi/J$, and δ_d vs the net current J divided by the emitter saturation current J_E.

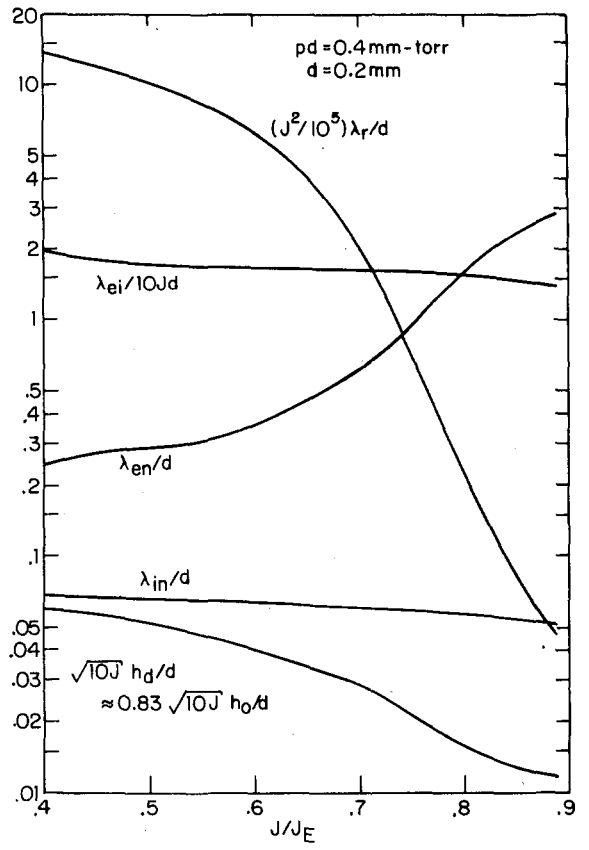

FIG. 7. Approximate values of mean free paths and Debye lengths vs J/J_E. Debye lengths were evaluated using the relation $h=(\theta_E/4\pi e^2 n_e)$.

perature T_C of 620°K, a pressure p of 2 Torr, and a range of values of current ratio J/J_E, current J, and the pressure-spacing product pd [determined by a chosen value of $\bar{d}$, defined by (44)]. The values of $\bar{d}$ investigated range between 20 and 100. The smallest value of the current ratio for which solutions were sought is 0.4; the upper limit of J/J_E was determined by a variety of numerical convergence problems. Values of J between 1 and 20 A/cm^2 were investigated.

Figure 6 indicates the cases for which $(\bar{R}_{ed}\phi)^2 \ll (5.4)^2$. Using this information, as discussed in Sec. IIIB, we can determine when many of the variables will either scale with or be entirely independent of J. In this figure and in all succeeding figures, the absence of an indication of the value of J for a curve implies independence of J for all applicable values of J.

A conservative estimate of the regions of applicability for all curves given here for which $pd=0.4$ mm Torr, in all figures in which a value of J is not indicated, is given in Fig. 6, according to which these curves are applicable to $1 \leq J \leq 20$ A/cm^2 for $0.4 \leq J/J_E \leq 0.65$, to $1 \leq J \leq 10$ A/cm^2 for $0.4 \leq J/J_E \leq 0.7$, and to $J=1$ A/cm^2 for $0.4 \leq J/J_E \leq 0.883$. We note that Fig. 6, in conjunction with (105) and Fig. 4 may be used to determine the form of S and the manner in which S^* is matched to S. Figure 6 also shows that $\bar{R}_{ed} > 1$, as required in order for the transport equations used to be valid for this analysis.

Figure 7 shows that $\lambda_{in} < \lambda_{en} \ll \lambda_{ei}$. Thus, most of the resistance to ambipolar diffusion is due to the neutrals and the value of λ_{in} is of primary importance in determining converter performance. Since, for small J/J_E, λ_{en} is less than an order of magnitude larger than λ_{in}, the value of λ_{en} may also be of some importance. The fact that the mean recombination length λ_r is much greater than any of the mean free paths indicates a nonequilibrium condition. The Debye lengths at the electrodes are seen to be much smaller than the interelectrode distance which is in agreement with our initial assumptions.

As predicted by the considerations of Sec. IVB, S^* is found to approximate S quite well for nonequilibrium cases $[(\bar{R}_{ed}\phi)^2 \ll (5.4)^2]$. In Figs. 8 and 9 we see distributions for two typical nonequilibrium cases. The values of the quantity $[\int_0^d (S^*-S)\,dx]/(\int_0^d S^*\,dx)$ in Figs. 8(a) and 9(a), which are used as a measure of how well S^* is fitted to S indicate good fits for both figures. For Fig. 8, $(\bar{R}_{ed}\phi)^2 \ll (5.4)^2$ for the entire range of J investigated. Thus, with the exception of Fig. 8(e), the curves in Fig. 8 are independent of J. By the same criterion, the independence of and scaling with J shown in Fig. 8, although not exploited in Fig. 9, apply to that figure for small values of J.

Figures 7, 8(g), 9(g), and 10 show that, except at small currents where $V_E < 0$ (the boundary conditions used assume an accelerating emitter sheath), the conditions required for (28) and (29) to apply are met. We therefore deduce from Fig. 10(b) that for $pd=0.4$ mm Torr, the boundary conditions used in this study are equivalent to the improved ones for J/J_E greater than about 0.65. It is difficult to estimate to what extent the solutions presented here for smaller J/J_E depart from those that would have been obtained had the improved boundary conditions been used. However, comparison of Figs. 8 and 9 shows that moderate variations in J/J_E in the vicinity of $J/J_E=0.65$ produce only moderate differences in the solutions. It is therefore felt that solutions for J/J_E not much smaller than 0.65 are acceptable.

Wilkins and McCandless[3] and Wilkins and co-workers[2], by means of a numerical "shooting" technique, have solved a set of transport equations which is essentially the same as ours using boundary conditions which, when the random current is greater than the directed current, are nearly the same as those of this study. The value for the ion-neutral cross section σ used in Refs. 2 and 3, 570 Å^2, is considerably smaller than ours.

One of the cases considered by Wilkins and McCandless[3] is suitable for comparison with the results presented here, although the conditions are somewhat different from ours. Their conditions are $T_E=1820$°K, $T_C=882$°K, $p=4$ Torr, $pd=0.6$ mm Torr, and $0 \leq J \leq 15$ A/cm^2. Due to the uncertainties involved in the use of the Richardson equation, the value of J_E is inferred from the results for the above case. It is found that the results of Wilkins and McCandless are in close agreement with ours if J/J_E for their work is taken to be 18 A/cm^2.

We observe many of the same trends in Fig. B-22 of Ref. 3 as in Fig. 10(b) of the present work. Their values of V_E, V_C, and ψ_d are all approximately the same as ours, but the values that they have obtained for these

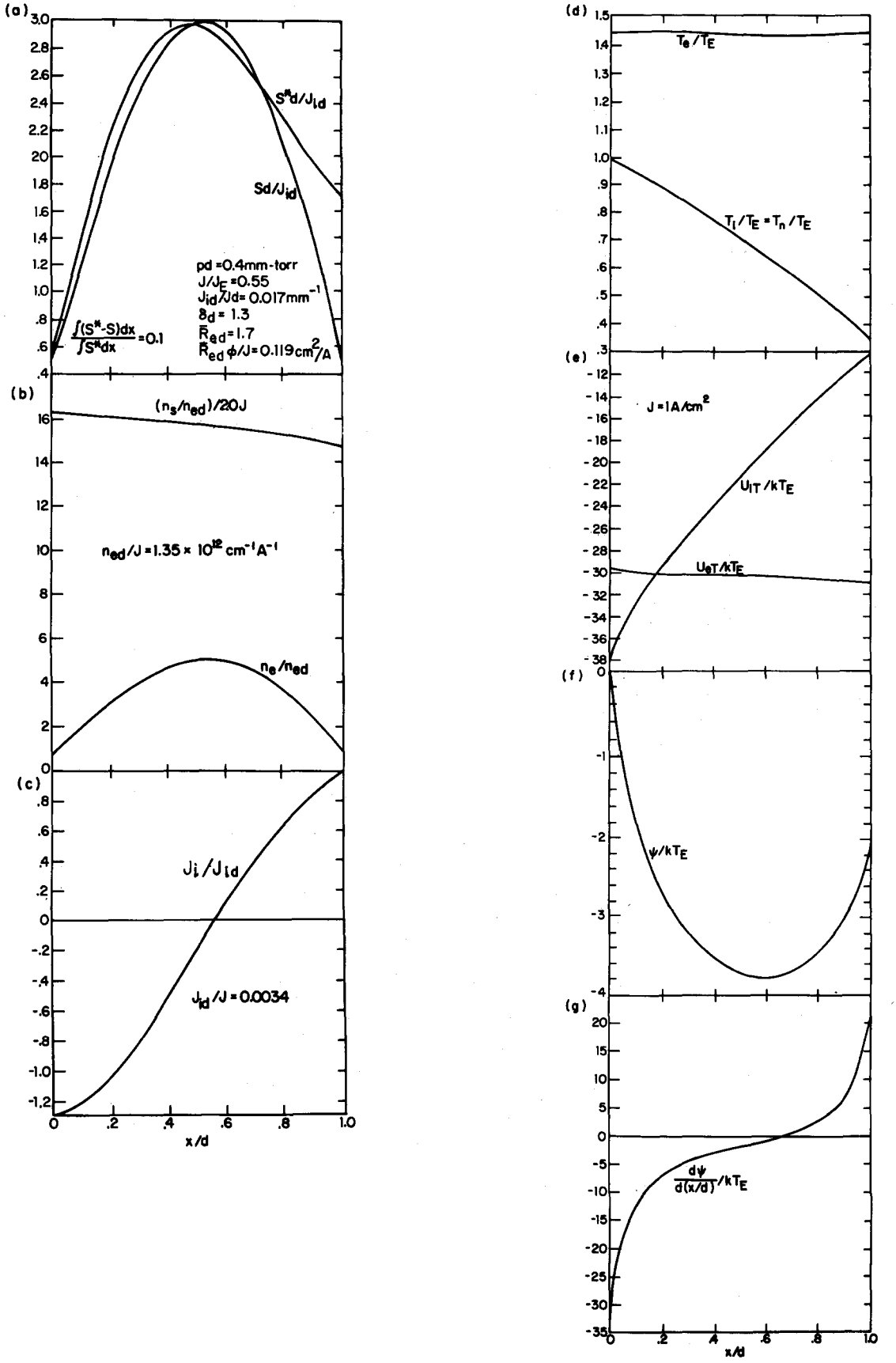

FIG. 8. Distributions for $J/J_E = 0.55$ and $1 \leq J \leq 20$ A/cm^2. $kT_E = 0.155$ eV.

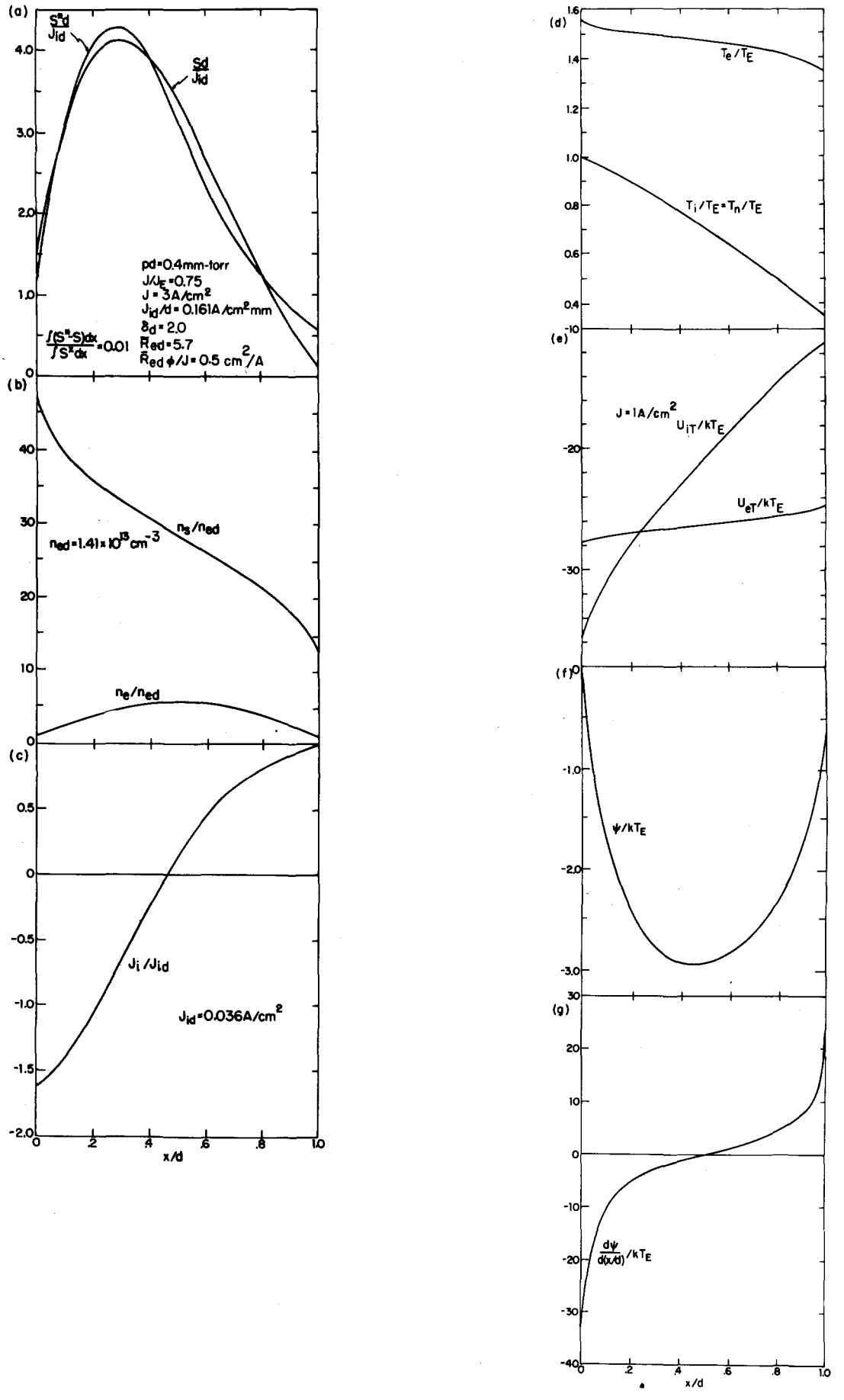

FIG. 9. Distributions for $J/J_E = 0.75$ and $J = 3$ A/cm^2. $kT_E = 0.155$ eV.

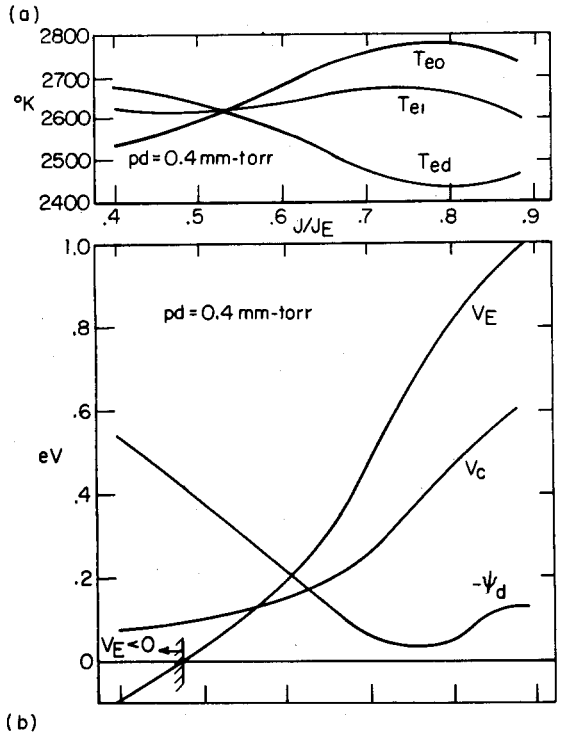

FIG. 10. (a) Electron temperature evaluated at the emitter, the collector, and the point of maximum electron production vs J/J_E. (b) Electrostatic sheath heights and electron potential distribution versus J/J_E.

variables show somewhat smaller slopes than ours when plotted against J/J_E as in Fig. 10(b).

It should be noted when considering the solutions presented in Refs. 2 and 3 that those solutions which exhibit a change in sign of the derivatives of the electrical potential between either of the sheaths and the adjacent edge of the plasma imply the existence of a double-valued sheath and are therefore unacceptable.

Comparison of Figs. 10(a), 8(d), and 9(d) with Fig. B-34 of Ref. 3 reveals a significant discrepancy in the results for the electron temperature. This difference can be traced to the relations used for the electron energy flux in the two studies. In their relation for Q_e, Wilkins and McCandless have $(\frac{3}{2}+\gamma_e)\theta_e$ in place of $\frac{5}{2}\theta_e$ in the convection term, where γ_e is the thermoelectric coefficient. With the variation in γ_e included, (7) may be written in the form

$$\theta_e = \left(\frac{Q_e}{\Gamma_e} - \psi\right)\left(\tfrac{3}{2}+\gamma_e - \frac{2\eta_e\mu_e}{\Gamma_e}\frac{d\theta_e}{dx}\right)^{-1}.$$

Wilkins and Gyftopoulos[4] found that for conditions similar to those of the present study $0.2 \leq \gamma_{ed} \leq 1.6$. Since the convection term is often much larger than the conduction term in (7), neglect of the variation in γ_e does have a noticeable effect on the value of θ_e. It is therefore felt by the authors that the differences between the two sets of results for θ_e are due primarily to the dependence of θ_e on γ_e. Another factor affecting the accuracy of θ_e in our results is contained in the assumption that a constant value for $(Q_e/\Gamma_e - \psi)$ may be used in the derivation of the relation for the electron temperature, (93).

Figures 8(b), 9(b), and 11, like Fig. 6, indicate nonequilibrium conditions. The values of n_e obtained by Wilkins and McCandless[3] are 2—3 times as large as ours for $J/J_E \approx 0.5$ and approximately the same as ours for $J/J_E \approx 0.8$ with the same qualitative variation in between. Since their distributions indicate greater values across the entire converter, by approximately the same amount across the entire converter, their values of n_e/n_{ed} are nearly the same as ours.

Comparison of the distributions of ion current density in Ref. 3 with those in Figs. 8(c) and 9(c) reveals somewhat smaller gradients in our curves with $J_i = 0$ at nearly the same point. In making the comparison, J_{id} in Ref. 3 is adjusted so as to correspond to $\sigma_{in} = 1200$ Å^2.

Figures 8(d) and 9(d) show that the distribution of T_e is somewhat nonlinear, particularly in the vicinity of the electrodes. Note that the ion temperature distribution, given by (2) and (30), is a function of the electrode temperatures only. As discussed above, our results for T_e do not agree well with those of Ref. 3.

From Figs. 8(e) and 9(e) we see that the total potentials, equal to the sum of the chemical and electrostatic potentials, vary nearly linearly across the converter. Comparison of Figs. 8(e) and 9(e) with Figs. 8(c) and 9(c) and Figs. 8(g) and 9(g) reveals the relative importance across the converter of the electrostatic and chemical potentials as sources of a driving force for diffusion.

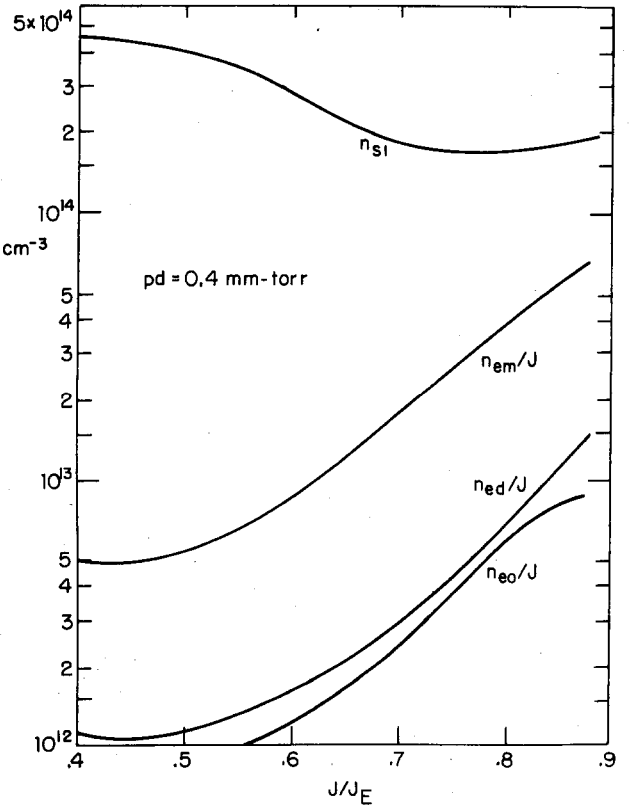

FIG. 11. Electron concentration at the emitter edge of the plasmas, n_{eo}, the collector edge of the plasma, n_{ed}, the point of maximum electron concentration, n_{em}, and the equilibrium electron concentration corresponding to the electron temperature at the point of maximum electron production, n_{si}, vs J/J_E.

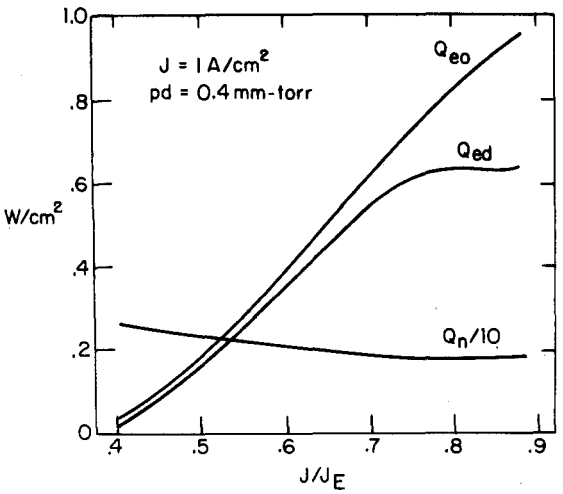

FIG. 12. The energy flux carried by the electrons evaluated at the plasma edges and by neutrals vs J/J_E. The heat flux carried by neutrals is independent of J.

The electrostatic potential, shown in Figs. 8(f) and 9(f), are found to have the same shape and a minimum at nearly the same position by Wilkins and McCandless[3] as in this study, although they find the variation to be somewhat less than we do. The electric field, given in Figs. 8(g) and 9(g), has large values in the vicinity of the electrodes, indicating high effective electrical resistivity in these regions.

In Fig. 12 we see that, since the energy flux carried by ions is negligible compared to that carried by neutrals, the neutrals transport most of the energy flux and the electrons transport a significant fraction of the total energy flux only for large values of J/J_E.

The variation of arc drop with pd is shown in Fig. 13. The present theory is the only one known to the authors which predicts the experimentally observed[18,19] minimum in V_D which we see here. The larger values of V_D at low pd exist because of low degrees of ionization due to loss of electrons to the walls by ambipolar diffusion. The larger values at high pd are due to the large resistance to diffusion in thick converters. It is found that pd increases with increasing $\bar{R}_{ed}\phi$ and that $\bar{R}_{ed}\phi = 5.4$ at a value of pd very near the minimum in V_D. Thus we have a single maximum in the ionization rate distribution and a good fit of S^* to S for pd less than 0.64 mm Torr and a second maximum in S develops as pd increases beyond this value. Note that this figure and Fig. 16 are the only ones which include cases in which there is anything but a good fit of S^* to S.

Kitrilakis *et al.*[18] plot the empirically observed variation of the arc drop with pd. That curve shows the minimum in V_D to occur at the same value of pd as in Fig. 13 and the slope of the V_D-pd curve for large pd to be the same as that observed here. Their values of V_D are larger than ours. Since the publication of Ref. 18, however, Rufeh and Lieb[19] have found that those values were too large; they found that at $pd = 0.25$ mm Torr, $V_D \approx 0.25$ eV and at $pd = 0.5$ mm Torr, $V_D \approx 0.2$ eV, as is shown in Fig. 13. This agrees very well with our results.

The current-voltage characteristics are shown in Fig. 14. The dashed lines are the double-sheath solutions discussed in Sec. IIIC. Since it is not known at what point a double sheath appears, a number of lines correspond-

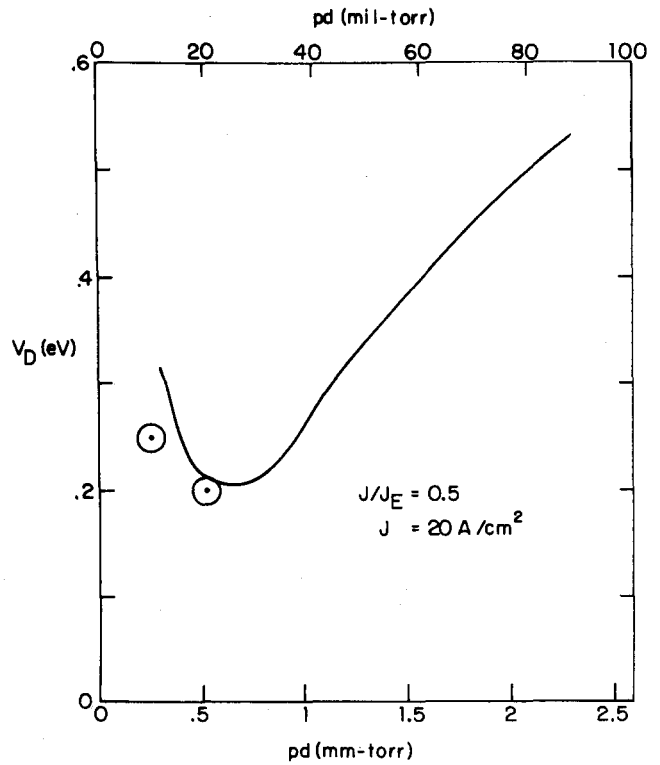

FIG. 13. The variation of the arc drop with the pressure-spacing product. Points marked ⊙ were determined experimentally by Rufeh and Lieb (Ref. 19).

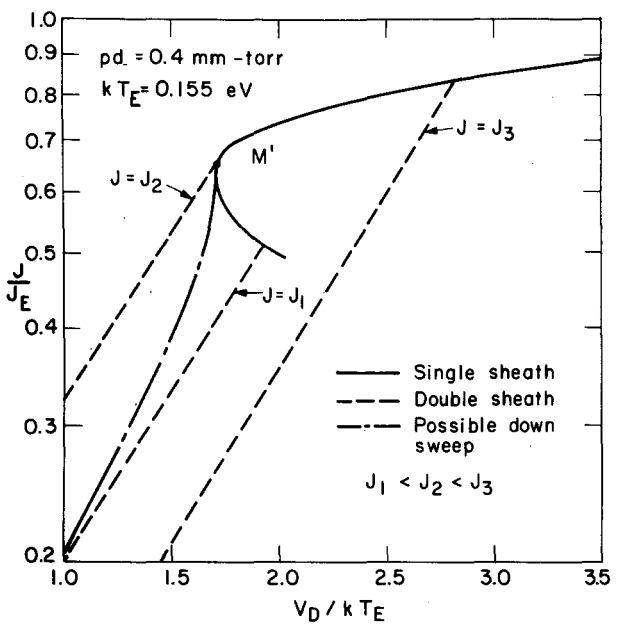

FIG. 14. Current-voltage characteristics J/J_E vs V_D/kT_E. The solid curve is the single-sheath solution. The dashed curves are double-sheath solutions for various values of J. The dot-dash curve is a possible downswing characteristic for a fixed value of J_E in the case where the double sheath forms at the point M'. To determine M' a criterion for double-sheath formation is required.

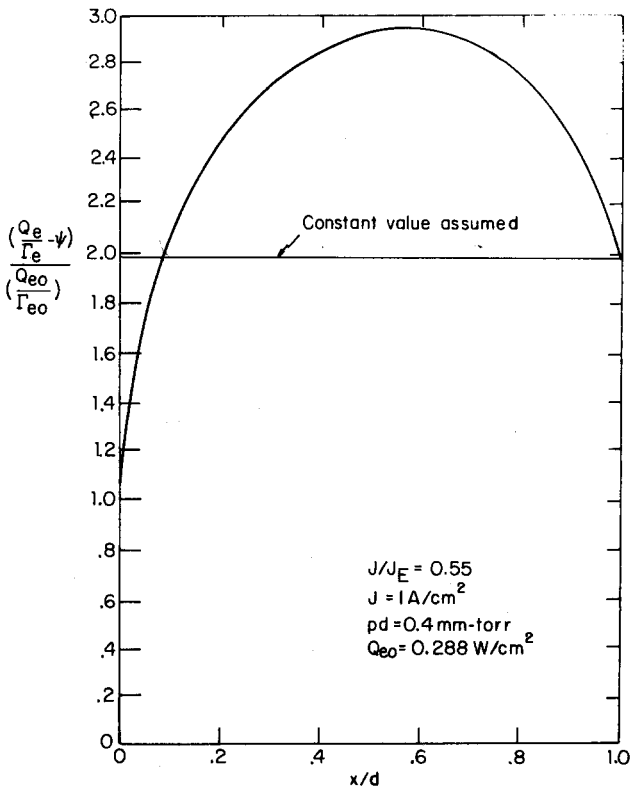

FIG. 15. Typical distribution of $(Q_e/\Gamma_e - \psi)$.

ing to various possibilities have been included. Note that each of these straight lines corresponds to a single value of J and varying J_E. Therefore, if a double sheath first appeared at point M' on the single-sheath curve, the remainder of the solution for constant J_E would take the form of the dot-dash line shown in the figure. To determine the point M' a criterion for double-sheath formation is required. This is not currently available.

B. Conclusions

The method presented here has proved highly accurate in comparison to other analytical methods and far simpler than the numerical "shooting" techniques. Furthermore, the equations derived provide greater qualitative insight into converter physics than can be obtained by numerical methods. However, some modification in the present method would result in very considerable enhancement of its usefulness.

A major factor limiting the accuracy of the present method is the assumption that $(Q_e/\Gamma_e - \psi)$ may be treated as a constant in the integration of the electron energy equation. Figure 15 shows a typical distribution of $(Q_e/\Gamma_e - \psi)$. We see that, although $(Q_e/\Gamma_e - \psi)$ is not constant, it does not vary over a very wide range, so the error introduced in using a constant value is probably not very great. In a future study, the variation in $(Q_e/\Gamma_e - \psi)$ can be accounted for by iteration or, alternatively, by numerical integration, as discussed in Sec. 7.

Allowing for variation in the thermoelectric coefficient, γ_e would also result in noticeable improvements in the values obtained for the electron temperature. It would, in addition, be of value to investigate whether accuracy might be improved by eliminating some of the other assumptions made in Sec. IIID.

The generality of the method can be increased by using the improved set of boundary conditions derived by Keck[12] and by using a more general assumed form for the electron production. In Fig. 16 we see S, S^*, and $(S - S^*)$ for a case in which S contains a double maximum. It is clear that $(S - S^*)$ can be represented by a function of the form of S^*. Thus, a general form of S^* can be obtained by superposing two forms of the type assumed here. It should be noted that the actual form for the ionization rate is likely to be somewhere between S and S^* in this figure.

The analysis could also be greatly simplified by exploiting the fact that the total potentials vary nearly linearly across the converter. In such a simplified analysis, it would be possible to obviate the large number of secondary approximations of the present method.

ACKNOWLEDGMENTS

This work was supported by the Thermo Electron Corporation of Waltham, Massachusetts. One of the authors (M. Ratafia) expresses his appreciation for support by an NDEA Fellowship.

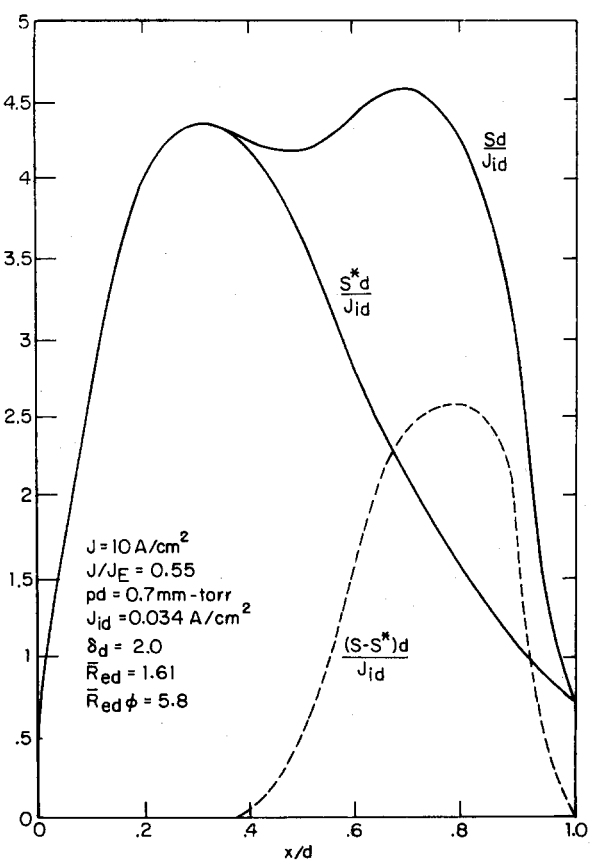

FIG. 16. Distributions of assumed and calculated ionization rates, S^* and S, and distribution of the difference between S^* and S.

*Present address: Harvard University, Division of Engineering and Applied Physics, 40 Oxford Street, Cambridge, Mass. 02138.

[1]D.R. Wilkins and E.P. Gyftopoulos, J. Appl. Phys. **7**, 2888 (1966).
[2]R.J. McCandless, D.R. Wilkins, and S.L. Derby, in *Conference Record of* 1969 *Thermionic Conversion Specialist Conference* (Institute of Electrical and Electronics Engineers, New York, 1969).
[3]D.R. Wilkins and R.J. McCandless, General Electric Company Report No. GESP-9004, 1969 (unpublished).
[4]D.R. Wilkins and E.P. Gyftopoulos, J. Appl. Phys. **7**, 2892 (1966).
[5]P. Mansbach and J. Keck, Phys. Rev. **181**, 275 (1969).
[6]E. Hinnov and J.G. Hirschberg, Phys. Rev. **125**, 795 (1962).
[7]R.W. Motley and A.F. Kuckes, in *Proceedings of the Fifth International Conference in Ionic Phenomena, Munich*, 1961 (North-Holland, Amsterdam, 1961).
[8]Yu. M. Aleskovskii, Zh. Eksperim. i Teor. Fiz. **44**, 840 (1963). [Soviet Phys.-JETP **17**, 570 (1963)].
[9]F.L. Mohler, J. Res. Natl. Bur. Std. (U.S.) **19**, 447 (1937).
[10]N. D'Angelo and N. Rynn, Phys. Fluids **4**, 1303 (1961).
[11]J.Y. Wada and R.C. Knechtli, Proc. IRE **49**, 1926 (1961).
[12]J. Keck (private communication).
[13]D.T. Shaw, in Ref. 2, p. 256.
[14]C. Warner and L.K. Hansen, in *Proceedings of the* 1967 *Thermionic Conversion Specialists Conference* (Institute of Electrical and Electronics Engineers, New York, 1967), p. 184.
[15]R.J. Anderson and W.L. Nighan, J. Appl. Phys. **41**, 3750 (1970).
[16]J.M. Houston, in *Report on the Thermionic Conversion Specialists Conference* (Institute of Electrical and Electronics Engineers, New York, 1964).
[17]The units of the total current J, wherever it appears in the figures, are A/cm^2. The total potentials, shown in Figs. 8(e) and 9(e), are given by $U_{eT} = U_{ech} + \psi$ and $U_{iT} = U_{ich} - \psi$. The chemical potential of species α, $U_{\alpha ch}$, is given by $U_{\alpha ch} = \theta_\alpha \ln[n_\alpha / 2(2\pi m_\alpha \theta_\alpha / h^2)^{3/2}]$.
[18]S.S. Kitrilakis, A. Shavit, and N.S. Rasor, in Annual Conference on Physical Electronics, MIT, 1964 (unpublished).
[19]F. Rufeh and D. Lieb, in Ref. 2, p. 237.